An efficient numerical scheme for the simulation of parallel-plate active magnetic regenerators

Bárbara Torregrosa-Jaime[a,*], José M. Corberán[a], Jorge Payá[a], Kurt Engelbrecht[b]

[a] Instituto de Ingeniería Energética (IIE), Universitat Politècnica de València

Camino de Vera s/n, Edificio 8E cubo F planta 5, 46022 Valencia, Spain

[b] Department of Energy Conversion and Storage, Technical University of Denmark

Frederiksborgvej 399, 4000 Roskilde, Denmark

Abstract

A one-dimensional model of a parallel-plate active magnetic regenerator (AMR) is presented in this work. The model is based on an efficient numerical scheme which has been developed after analysing the heat transfer mechanisms in the regenerator bed. The new finite difference scheme optimally combines explicit and implicit techniques in order to solve the one-dimensional conjugate heat transfer problem in an accurate and fast manner while ensuring energy conservation. The present model has been thoroughly validated against passive regenerator cases with an analytical solution. Compared to the fully implicit scheme, the proposed scheme achieves more accurate results, prevents numerical errors and requires less computational effort. In AMR simulations the new scheme can reduce the computational time by 88%.

Keywords: Regenerator; Modelling; Simulation; Magnetic refrigerator; Finite differences

**Corresponding author*. Tel: +34 963879122; Fax: +34 963877272;

E-mail address: bartorja@iie.upv.es (B. Torregrosa-Jaime)

NOMENCLATURE

A_c	Total cross-sectional area [m^2]	Δt	Time step length [s]
a_s	Specific surface area [m^2 m^{-3}]	v	Fluid velocity [m s^{-1}]
CFL	$v\Delta t/\Delta x$, Courant-Friedrichs-Lewy condition [-]	W	Regenerator width [m]
c	Specific heat capacity [J K^{-1} kg^{-1}]	x	Bed location [m]
d_h	Hydraulic diameter [m]	Δx	Spatial node length [m]
E	Energy [J]		
Ec	Eckert number [-]	*Greek symbols*	
f	Friction factor [-]	α	Thermal diffusivity [m^2 s^{-1}]
H	Regenerator height [m]	δ	Energy conservation error [-]
h	Convection coefficient [W K^{-1} m^{-2}]	ε	Porosity [-]
k	Thermal conductivity [W K^{-1} m]	ρ	Density [kg m^{-3}]
L	Regenerator length [m]	μ	Viscosity [Pa s^{-1}]
$\dot{m}$	Mass flow rate [kg s^{-1}]	$\mu_0 H$	Magnetic field [T]
Nt	Number of time steps [-]		
Nu	Nusselt number [-]	*Subscripts*	
Nx	Number of spatial nodes [-]	app	Applied
p	Pressure [Pa]	C	Cold reservoir
Pe	Péclet number [-]	f	Fluid
$\dot{Q}$	Heat load [W]	H	Hot reservoir
$\dot{q}$	Heat flux [W m^{-2}]	i	Spatial node number
s	Specific entropy [J K^{-1}]	MCE	Magnetocaloric effect
T	Temperature [K]	r	Solid regenerator material
t	Time [s]	0	Initial

1. Introduction

Regenerative heat exchangers cyclically store heat from a hot fluid in order to release it to a cold fluid. These devices are useful for recovering thermal energy in a number of applications such as air-conditioning systems, industrial stoves and gas turbines. Due to its interest, many authors have developed closed solutions to rapidly evaluate the performance of heat regenerators in their cyclic steady state. These solutions can be classified regarding the consideration of heat conduction in the solid matrix or the entrained fluid heat capacity (Klein and Eigenberger, 2001). To the knowledge of the authors, there is no closed solution including both effects at a time, so in this case it is necessary to employ numerical methods.

Recently, regenerative heat exchangers have found a new application in magnetic refrigeration at room temperature (Romero Gómez et al., 2013). Active magnetic regenerator (AMR) refrigerators consist of a solid matrix made of a magnetocaloric material (MCM) traversed by a fluid which flows alternatively from the cold end to the hot end of the regenerator synchronized with the magnetization of the MCM. Several assumptions applied in conventional passive regenerator models are not valid for AMRs. The heat transfer fluid in AMRs is usually a liquid so its heat capacity is not negligible (Nellis and Klein, 2006). The thermal conductivity of typical MCMs such as gadolinium is also significant (Nielsen and Engelbrecht, 2012). Moreover, the properties of the MCMs vary with the magnetic field and temperature. Several authors have developed numerical models in order to predict the AMR performance (Nielsen et al., 2011). In the case of parallel-plate regenerators, 1D models achieve accurate results with a reasonable computation time (Petersen et al., 2008).

The numerical technique employed to solve the regenerator equations is decisive in minimizing numerical errors, instability and computational effort. However, few authors of AMR models specify which numerical approach they employ. Engelbrecht (2008), Oliveira et al. (2012) and Tušek et al. (2011) apply the finite differences method with an implicit scheme while Nikkola et al. (2014) employ an explicit scheme and Nielsen et al. (2009) adopt the ADI method. On the other hand, Petersen (2007) and Dikeos and Rowe (2013) employ a finite element approach. To the authors' knowledge, the suitability of the different numerical techniques in AMR applications has not been analysed yet in depth.

In this work, a new 1D model of a parallel-plate AMR is presented. The model is based on a new numerical scheme adapted to the most relevant heat transfer processes that occur in the regenerator bed. In particular, the scheme optimally combines an explicit scheme for the fluid part of the regenerator with an implicit scheme for the solid part. The new scheme is therefore named Hybrid Explicit-Implicit Scheme (HEIS). The scheme is thoroughly validated against special passive regenerator cases where an analytical solution is available. Several hypotheses and numerical techniques are compared in terms of accuracy, computational time and numerical errors. The results obtained are interesting not only for AMR applications, but also for the efficient simulation of conventional parallel-plate regenerators.

2. Model description

The modelled AMR consists of a stack of equally spaced parallel plates made of an MCM subjected to a time-dependent fluid flow and limited by a cold and a hot reservoir at T_C and T_H temperatures respectively (Fig. 1). The model calculates the temperature of the fluid ($T_f(x,t)$) and the solid ($T_r(x,t)$) parts of the regenerator in the flow direction at each moment of the AMR cycle. The inputs to the model are the fluid mass flow rate ($\dot{m}(t)$) at the entrance of the corresponding reservoir and the internal magnetic field ($\mu_0 H(x,t)$). The internal magnetic field depends on the applied magnetic field, on the magnetic properties of the regenerator and on its temperature. For the sake of simplicity, the internal magnetic field is calculated by means of a demagnetization model which is independent of the AMR model, assuming a linear temperature profile in the regenerator. (Engelbrecht et al., 2013).

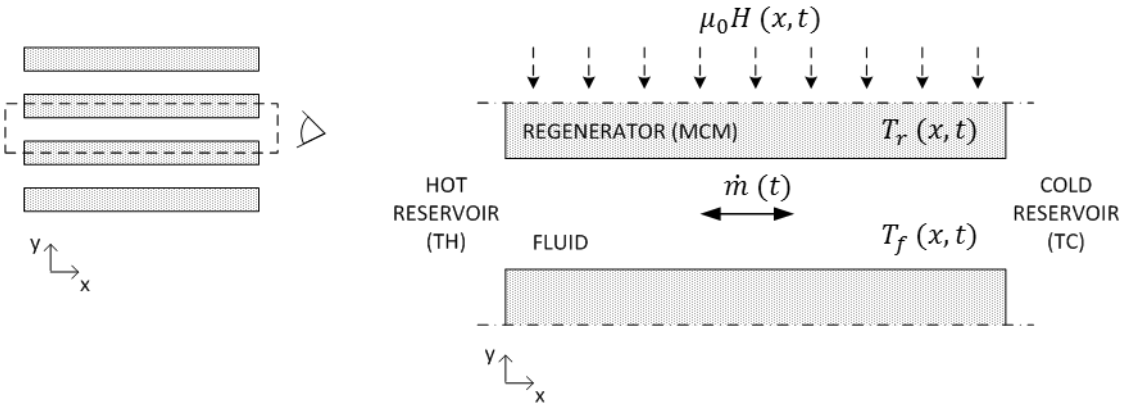

Fig. 1. Scheme of the 1D parallel-plate AMR model.

The governing equations that describe the change in temperature of the system are obtained from energy balances in the fluid (Eq. 1) and in the solid (Eq. 2).

$$\varepsilon A_c \rho_f c_f \frac{\partial T_f}{\partial t} = -v\varepsilon A_c \rho_f c_f \frac{\partial T_f}{\partial x} + \varepsilon A_c k_f \frac{\partial^2 T_f}{\partial x^2} + h a_s A_c \left(T_r - T_f\right) + \frac{\partial p}{\partial x}\frac{\dot{m}}{\rho_f} \qquad (1)$$

$$(1-\varepsilon) A_c \rho_r c_r \frac{\partial T_r}{\partial t} = (1-\varepsilon) A_c k_r \frac{\partial^2 T_r}{\partial x^2} + h a_s A_c \left(T_f - T_r\right) + (1-\varepsilon) A_c \dot{q}_{MCE} \qquad (2)$$

In Eq. (1), the term on the left hand side represents the energy storage in the fluid. On the right hand side, the first term is the advection term, the second describes the axial conduction, the third accounts for the convective heat transfer between the fluid and

the solid and the fourth, for the heat generation due to viscous dissipation. The fluid is assumed to be incompressible.

Similarly, in Eq. (2) the left-hand-side term describes the energy storage in the regenerator bed. On the right hand side, the first term accounts for the axial conduction, the second represents the convective heat transfer between the fluid and the solid and the third, the magnetocaloric effect. Heat losses to the ambient are neglected in this study because the aim is to validate the new scheme with analytical solutions and not with experimental results of a given device.

Eqs. (1-2) are solved numerically with the finite differences method in a single channel which is assumed to be representative of the entire stack. The numerical solution is calculated at the centre of each control volume defined by a spatial grid along the regenerator length (Fig. 2). This approach enables the definition of a conservative scheme.

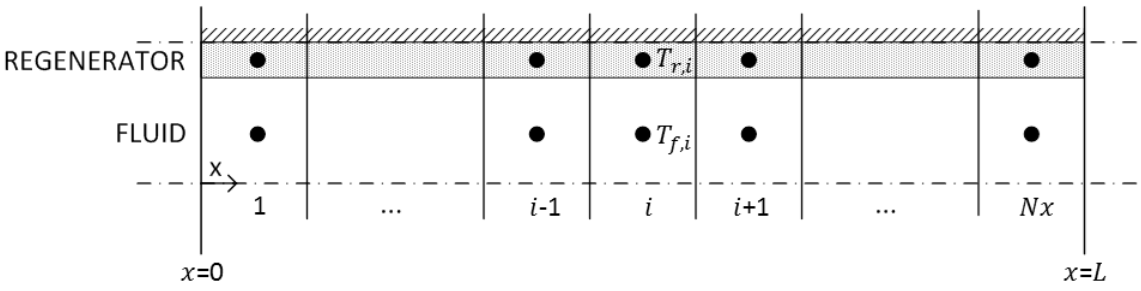

Fig. 2. Discretization and nomenclature used in the numerical model.

2.1. Fluid equation

Advection problems are solved best by explicit techniques due to the hyperbolic character of the partial differential equations that describe them. However, diffusion problems have elliptic character and hence require an implicit treatment. Consequently, the most suitable numerical scheme to solve Eq. (1) depends on the relative importance of each term, which in a first approach can be estimated with the Péclet number, $Pe = vL/\alpha$.

Pe is obtained from the analytical solution of the convection-diffusion equation in steady state. Diffusion is negligible if Pe is greater than 100. Considering the most limiting AMR parameters found in recent literature (v=0.06 cm s^{-1}, L=40 mm, α=1.23·10^{-7} m^2 s^{-1} (Bahl et al., 2008)), a value of Pe = 196 is obtained. Most of the published AMR devices work with fluid velocities one and two orders of magnitude larger, so in a typical AMR Pe is expected to be greater than 1000. Therefore, axial thermal conduction in the

fluid can be neglected. This hypothesis will be verified in section 3.4 considering all the terms in Eq. (1).

The importance of the viscous dissipation term in the change of the fluid temperature can be checked with the Eckert number, $Ec = v^2/c_p\Delta T$, where ΔT is the boundary layer temperature difference (Incropera et al., 2007). Considering the highest flow speed found in AMR literature (v=36.7 cm s^{-1} (Trevizoli et al., 2011)), assuming ΔT=2 K and a mixture of water and glycol as the heat transfer fluid, a value of Ec≈2·10^{-5} is obtained. Since Ec is much lower than 1, it can be concluded that the viscous dissipation term is negligible in AMR operating conditions studied here. However, viscous dissipation may have a cumulative effect after a large number of cycles and may become important given that the current trend in AMRs is to employ a reduced channel spacing (Tušek et al., 2013). Therefore, the viscous dissipation term is finally included in the fluid energy equation as a source term, as explained below.

If conduction in the fluid is neglected, an explicit scheme can be applied to discretize Eq. (1). A second order scheme has been developed, since first order schemes produce diffusion when the exact solution cannot be found numerically. In order to ensure the energy conservation, Eq. (1) can be expressed in Eq. (3) as a flow-based energy balance for each control volume.

$$\frac{d}{dt}\int_{i-\frac{1}{2}}^{i+\frac{1}{2}} \varepsilon A_c \rho_f c_f T_f(x,t)dx = v\varepsilon A_c \rho_f c_f \left[T_f\left(x_{i-\frac{1}{2}},t\right) - T_f\left(x_{i+\frac{1}{2}},t\right)\right] + \int_{i-\frac{1}{2}}^{i+\frac{1}{2}} h a_s A_c \left[T_r(x,t) - T_f(x,t)\right]dx + \int_{i-\frac{1}{2}}^{i+\frac{1}{2}} \frac{\partial p}{\partial x}\frac{|\dot{m}|}{\rho_f}dx \quad (3)$$

Eq. (3) is the energy balance when the fluid flows from the hot to the cold reservoir as illustrated in Fig. 1 (v>0). The expression for v<0 is analogous.

Assuming constant fluid properties and a constant convection coefficient (h) during a time step and considering that the temperature at the centre of the control volume (T_i) equals the mean temperature in the control volume i ($\bar{T}_i$), which is defined in Eq. (4),

$$T_i = \bar{T}_i = \frac{\int_{i-\frac{1}{2}}^{i+\frac{1}{2}} T(x,t)dx}{\Delta x} \quad (4)$$

the value of the temperature of the fluid is found by substituting Eq. (4) into Eq. (3) and integrating over the time step (Eq. 5). The viscous dissipation term has been expressed more conveniently by employing the friction factor (Incropera et al., 2007).

$$\bar{T}_{f,i}^{n+1} - \bar{T}_{f,i}^{n} = \int_{t^n}^{t^{n+1}} d\bar{T}_{f,i}$$
$$= \frac{v}{\Delta x}\int_{t^n}^{t^{n+1}} \left[T_f\left(x_{i-\frac{1}{2}}, t\right) - T_f\left(x_{i+\frac{1}{2}}, t\right)\right] dt + \frac{h a_s}{\varepsilon \rho_f c_f}\int_{t^n}^{t^{n+1}} \left(\bar{T}_{r,i} - \bar{T}_{f,i}\right) dt$$
$$+ \frac{f|v^3|}{2 d_h c_f}\Delta t \qquad (5)$$

In the first term of the right-hand side of Eq. (5), the values of the temperatures at the boundaries of the control volume ($T_f\left(x_{i-1/2}, t\right)$ and $T_f\left(x_{i+1/2}, t\right)$) are calculated by considering the change in temperature due to the incoming flow (advection) plus the effect of the heat transfer with the solid (convection) (Fig. 3). Viscous dissipation is neglected at this point.

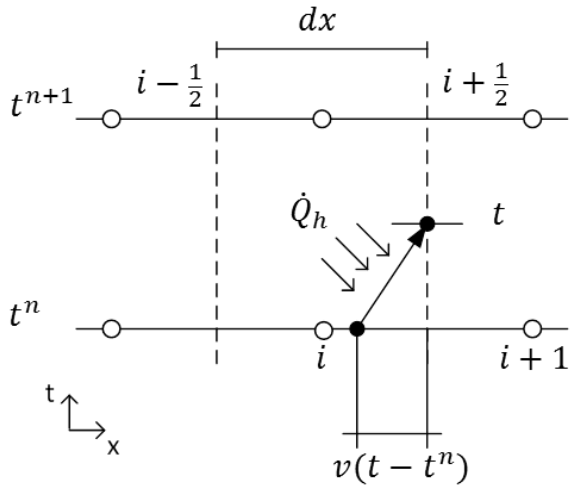

Fig. 3. Path followed by a fluid particle during a time step.

The advection term is solved explicitly. The exact solution of the transport equation can be found numerically only when the distance that a particle travels in one time step equals the distance between two adjacent spatial nodes. In other words, when $CFL = v\Delta t/\Delta x = 1$. If CFL <1, then $x_i - v\Delta t$ is not defined in the spatial grid, so a linear distribution of the fluid temperature inside each cell i at each time step n is assumed (Eq. 6). This definition is consistent with Eq. (4).

$$T_f(x, t^n) = \bar{T}_{f,i}^{n} + (x - x_i)\,\sigma_{f,i}^{n} \qquad (6)$$

With the purpose of minimizing the numerical diffusion (section 3.1), the MC Limiter approach (Van Leer, 1977) was chosen to calculate the slope of the temperature distribution ($\sigma_{f,i}^{n}$).

Regarding the convection term, different hypotheses were tested to calculate heat transfer with the regenerator:

- Hypothesis 1 (HEIS1): constant heat flux. $\Delta T = \bar{T}_{r,i}^{n} - \bar{T}_{f,i}^{n}$ is constant.
- Hypothesis 2 (HEIS2): constant heat flux. $\Delta T = T_{r,i,0}^{n} - T_{f,i,0}^{n}$ is constant, where subscript 0 indicates that $T_{r,i}$ and $T_{f,i}$ are calculated at the beginning of the time step.
- Hypothesis 3 (HEIS3): the temperature of the solid varies slowly. $T_{r,i}^{n} = \bar{T}_{r,i}^{n}$ is constant.
- Hypothesis 4 (HEIS4): the temperature of the solid has a linear distribution in each cell analogous to Eq. (6).

In the second term of the right-hand side of Eq. (5), the integral of $\bar{T}_i^n$ can be approached numerically by different techniques. Eq. (7) was programmed with the purpose of applying the implicit method (m=1), the Crank-Nicholson method (m=0.5) and the explicit method (m=0).

$$\int_{t^n}^{t^{n+1}} \bar{T}_i dt = [(1-m)\bar{T}_i^n + m\bar{T}_i^{n+1}]\Delta t \tag{7}$$

Eq. (5) is discretized by developing and substituting the previous hypotheses. The boundary condition is that the fluid enters the regenerator at the temperature of the corresponding reservoir.

2.2. Regenerator equation

The regenerator equation is formulated in an analogous way to the fluid equation so they can be both coupled. Eq. (2) is expressed as a flow-based energy balance (Eq. 8). The heat gain due to the magnetocaloric effect is treated as the magnetic-field driven change in the regenerator entropy (Engelbrecht, 2008).

$$\begin{aligned}\frac{d}{dt}\int_{i-\frac{1}{2}}^{i+\frac{1}{2}} (1-\varepsilon)A_c\rho_r c_r T_r(x,t)dx \\ = -k_r(1-\varepsilon)A_c\left[\frac{2T_r(x_i,t) - T_r(x_{i-1},t) - T_r(x_{i+1},t)}{\Delta x}\right] \\ - \int_{i-\frac{1}{2}}^{i+\frac{1}{2}} h a_s A_c\left[T_r(x,t) - T_f(x,t)\right]dx \\ - \int_{i-\frac{1}{2}}^{i+\frac{1}{2}} (1-\varepsilon)A_c\rho_r T_r(x,t)\frac{\partial s_r}{\partial \mu_0 H}_T \frac{\partial \mu_0 H}{\partial t}dx\end{aligned} \tag{8}$$

The regenerator properties are assumed to be constant during a time step. If the definition in Eq. (4) is employed and the time derivative of the magnetic field is approximated by applying the mean value theorem, Eq. (9) is obtained by integrating Eq. (8) over the time step.

$$\bar{T}_{r,i}^{n+1} - \bar{T}_{r,i}^{n} = \int_{t^n}^{t^{n+1}} d\bar{T}_{r,i}$$
$$= \frac{k_r}{\rho_r c_{r,\mu_0 H} \Delta x^2} \int_{t^n}^{t^{n+1}} \left(\bar{T}_{r,i+1} - 2\bar{T}_{r,i} + \bar{T}_{r,i-1}\right) dt + \frac{h a_s}{(1-\varepsilon)\rho_r c_r} \int_{t^n}^{t^{n+1}} \left(\bar{T}_{r,i} - \bar{T}_{f,i}\right) dt$$
$$- \frac{1}{c_r} \frac{\partial s_r}{\partial \mu_0 H_T} \left[\frac{\mu_0 H_i^{n+1} - \mu_0 H_i^{n}}{\Delta t}\right] \int_{t^n}^{t^{n+1}} \bar{T}_{r,i} dt \qquad (9)$$

Eq. (9) is discretized by employing Eq. (7). The ends of the regenerator are assumed to be adiabatic.

2.3. Numerical solution algorithm

Eqs. (5) and (9) in their discretized forms constitute a system of linear equations. Eq. (5) is substituted into Eq. (9) so the latter is solved efficiently with the tri-diagonal matrix algorithm (TDMA). The present model has been implemented in MATLAB.

3. Results and discussion

The proposed model has been validated in the limit of several ideal passive regenerator cases with an analytical solution. Afterwards, it has been employed to simulate both the oscillating passive regenerator and the AMR under typical working conditions. The simulation results are compared to those of the implicit model developed by Engelbrecht (2008).

3.1. Transport equation

The scheme proposed for the advection term of the fluid equation (Eq. 5) is analysed in this section. Only the fluid portion of the regenerator is simulated. The convective, conductive and viscous dissipation effects are not considered with the purpose of focusing only on advection.

The analytical solution of the transport equation considering only advection in the fluid has been compared with the proposed scheme and with the implicit scheme. A stepwise variation of the temperature of the fluid flow at the inlet of the channel was simulated with the parameters in Table 1 and Nx=100.

Parameter	Value	Parameter	Value
$\boldsymbol{T_H}$	30 K	$\boldsymbol{T_0}$	0 K
$\boldsymbol{\rho_f}$	1000 kg m^{-3}	$\boldsymbol{\rho_r}$	8900 kg m^{-3}
$\boldsymbol{c_f}$	4200 J kg^{-1} K^{-1}	$\boldsymbol{c_r}$	500 J kg^{-1} K^{-1}
$\boldsymbol{\dot{m}}$	0.005 kg s^{-1}	$\boldsymbol{A_C}$	0.001 m^2
$\boldsymbol{L}$	1 m	$\boldsymbol{\varepsilon}$	0.36

Table 1. Parameters employed in the model validation (Engelbrecht, 2008).

Fig. 4 shows the calculated fluid temperatures along the channel at several moments of the simulation with different values of CFL. The proposed scheme (HEIS) minimizes numerical diffusion with respect to the implicit scheme (IMP) when the model is executed with values of CFL close to 1 (Fig. 4a). In fact, since the advection term is solved explicitly in the presented scheme, the exact solution is achieved when CFL =1. If very low values of CFL are used, the proposed scheme still resembles the analytical solution while the implicit scheme produces oscillations (Fig. 4b).

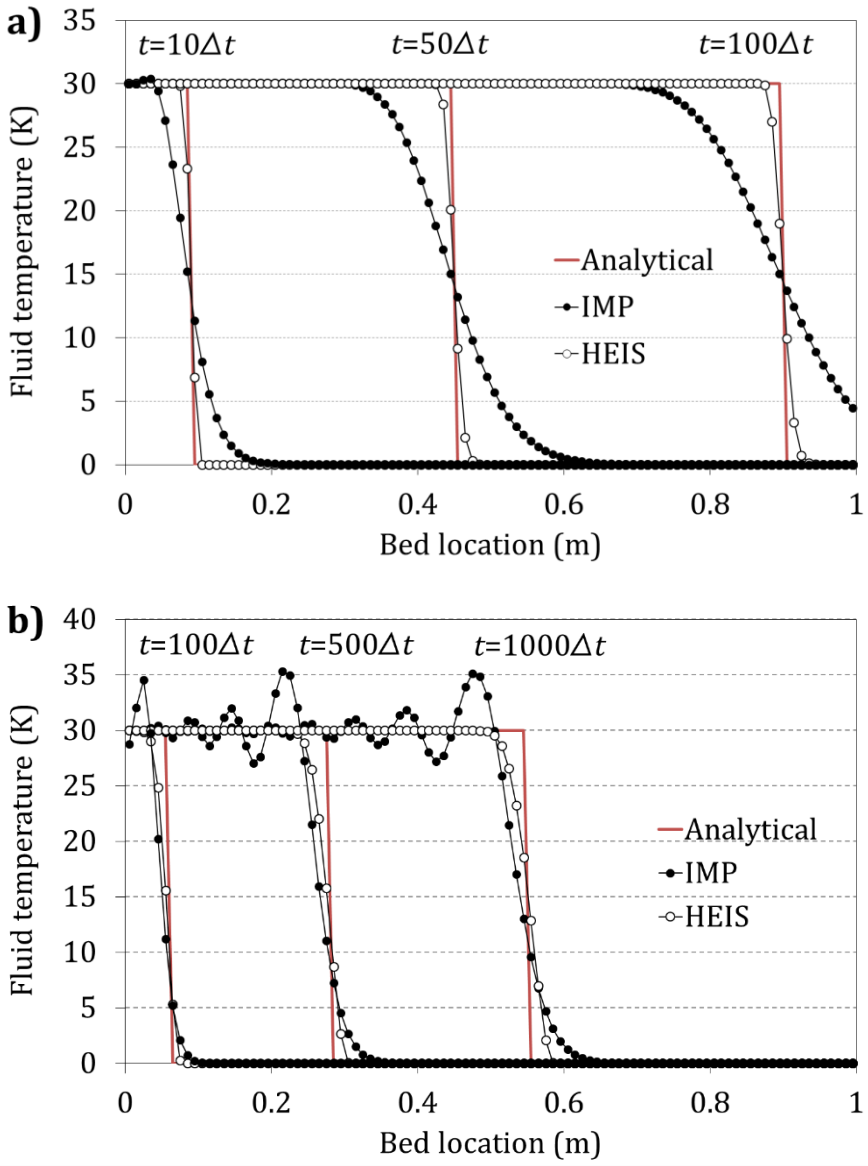

Fig. 4. Fluid temperature predicted by the models and analytical solution of the transport equation with a) CFL=0.9 b) CFL<<1.

3.2. Single-blow ideal passive regenerator

The model results have been compared with the Schumann solution for a single-blow transient passive regenerator with no axial conduction (Shitzer and Levy, 1983). As by Engelbrecht (2008), the simulation has been run with a flow period of 100 s, NTU=50 and the parameters in Table 1.

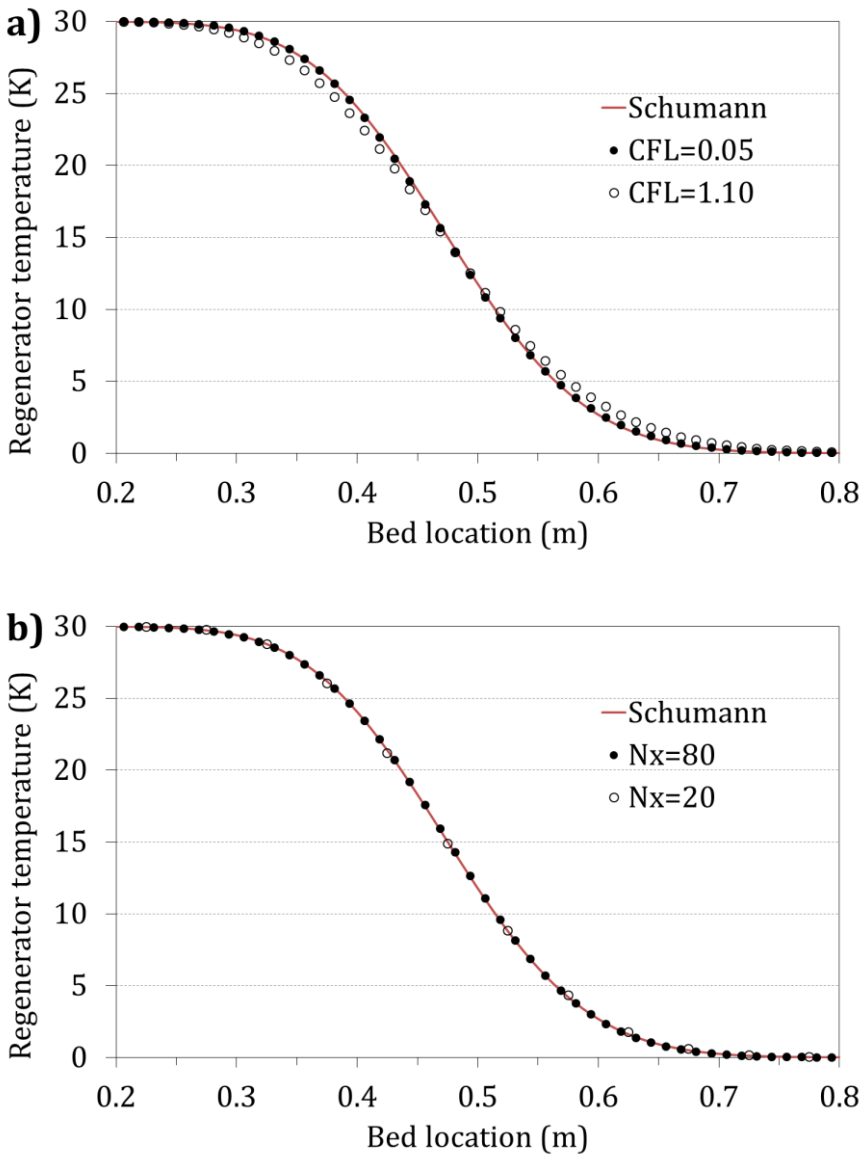

Fig. 5. Regenerator temperature predicted by the Schumann solution, a) the implicit model (Engelbrecht, 2008) and b) the present model HEIS1 m=1.

The implicit scheme reproduces the Schumann solution with Nx=80 provided that the number of time steps (Nt) is high enough (Engelbrecht, 2008) (Fig. 5a). On the contrary, the proposed model achieves the Schumann solution with CFL as large as 0.99, which corresponds to the minimum time step possible for the developed scheme. Moreover, the number of spatial nodes can also be reduced (Fig. 5b). These results are achieved with the approaches HEIS1 and HEIS2 combined with m=1 and m=0.5. Approaches HEIS3 and HEIS4 behave like the implicit scheme and m=0 produces oscillations at the wave front, so they were not further investigated.

Table 2 compares the results obtained with the proposed model (HEIS) and the implicit model (IMP) in terms of accuracy, energy conservation error and computation time. The

accuracy is determined with the root mean squared error ($RMSE$) taking as a reference the Schumann solution (Eq. 10). The energy conservation error (δ) is expressed as the total energy variation along the calculation minus the energy difference between the final and the initial states (Eq. 11).

$$RMSE = \frac{\sqrt{\sum_i^N \left(T_{ref,i} - T_{sim,i}\right)^2}}{N} \tag{10}$$

$$\delta = \frac{\int_0^t \Delta E - \left(\int_0^L E_t - \int_0^L E_0\right)}{\int_0^L E_t - \int_0^L E_0} \tag{11}$$

Scheme	$\boldsymbol{CFL}$	$\boldsymbol{Nx}$=80			$\boldsymbol{Nx}$=20		
		$\boldsymbol{RMSE\ T_r}$ (K)	$\boldsymbol{\delta}$ (%)	$\boldsymbol{t}$ (s)	$\boldsymbol{RMSE\ T_r}$ (K)	$\boldsymbol{\delta}$ (%)	$\boldsymbol{t}$ (s)
IMP	1.10	0.0503	$6.5\cdot10^{-8}$	0.2172	0.3668	$3.8\cdot10^{-5}$	0.0216
IMP	0.05	0.0086	$1.7\cdot10^{-10}$	3.9776	0.2299	$2.2\cdot10^{-7}$	0.2627
HEIS1 $\boldsymbol{m}$=1	0.99	0.0037	$3.0\cdot10^{-11}$	0.0831	0.0183	$4.9\cdot10^{-9}$	0.0089
HEIS1 $\boldsymbol{m}$=0.5	0.99	0.0008	$1.4\cdot10^{-10}$	0.0827	0.0253	$1.2\cdot10^{-10}$	0.0086
HEIS2 $\boldsymbol{m}$=1	0.99	0.0060	$1.6\cdot10^{-12}$	0.0124	0.0527	$-5.6\cdot10^{-8}$	0.0023
HEIS2 $\boldsymbol{m}$=0.5	0.99	0.0032	$1.7\cdot10^{-11}$	0.0130	0.0804	$-1.6\cdot10^{-8}$	0.0023

Table 2. Single-blow ideal regenerator simulation results of the proposed model (HEIS) and the implicit model (IMP).

The proposed model approaches more accurately the Schumann solution than the implicit model, particularly if less spatial nodes are employed. The energy conservation error and therefore the numerical dispersion are lower with the presented scheme due to the larger CFL which is employed, as discussed in section 3.1. With respect to the IMP-CFL=0.05 case, the proposed model reduces significantly the simulation time due to the increase in the time step and to the efficiency of the TDMA.

In general, HEIS1 is more accurate than HEIS2. The results of HEIS2 may be improved by changing the definition of the slope of the temperature distribution in the regenerator. However, HEIS1 already achieves a good compromise so it has been finally chosen among the four proposed approaches.

3.3. Oscillating ideal passive regenerator

The model has also been validated against the solution of an oscillating passive regenerator with no entrained fluid heat capacity and no axial conduction. Dragutinovic and Baclic (1998) calculated the effectiveness of this regenerator at the cyclical steady state as a function of the number of transfer units (NTU) and the utilization ($U = \bar{\dot{m}} c_f \tau / (2A_c L(1-\varepsilon)\rho_r c_r)$) using an oscillating rectangular mass flow rate variation of magnitude $\bar{\dot{m}}$ and period τ. The hypothesis of no entrained fluid capacity can be simulated with the AMR model by setting the porosity ε very close to 0. The steady state is reached when the change in the regenerator temperatures from cycle to cycle remains below 10^{-5}. Engelbrecht (2008) reported these results and found an excellent agreement with the calculations by his implicit model with Nx=100 and Nt=3000. In Fig. 6 the results by Engelbrecht (2008) are compared to the ones of the proposed model, which predicts practically the same values with Nx=20 and CFL≈1.

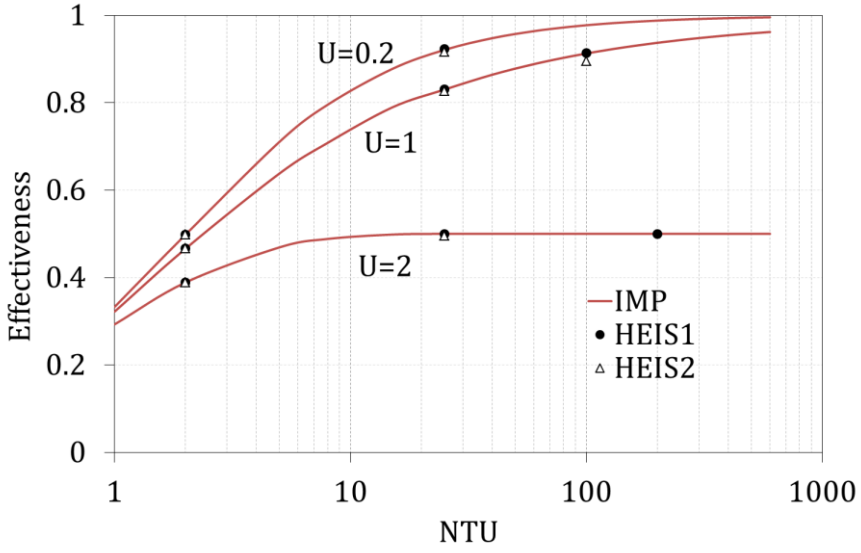

Fig. 6. Effectiveness of the oscillating ideal passive regenerator predicted by the implicit (IMP) and the proposed (HEIS) models

In fact, both models predict a similar temperature distribution inside the regenerator (Fig. 7). However, in the regions where the convective heat transfer is very low the implicit scheme produces small oscillations due to the low CFL employed. On the contrary, the proposed scheme preserves monotonicity.

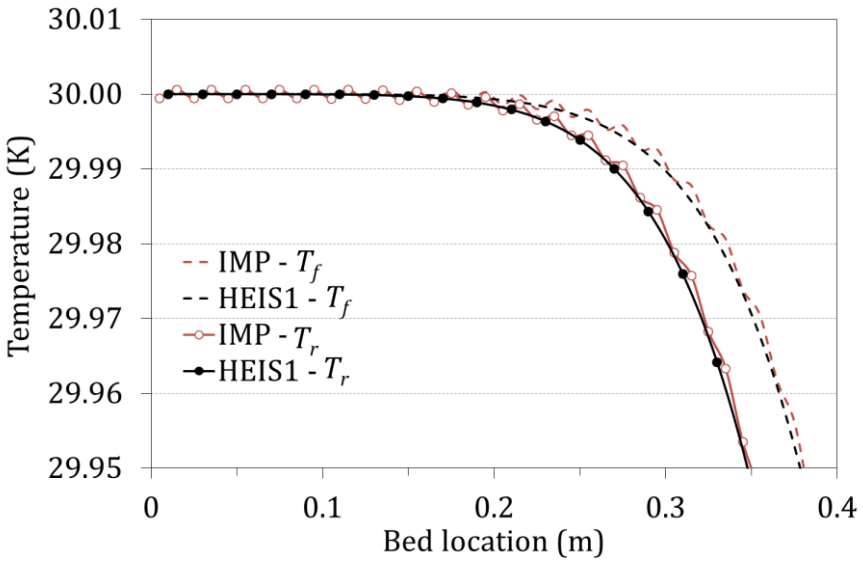

Fig. 7. Simulated temperature profiles at the cyclical steady state (U=1, NTU=25).

3.4. Oscillating passive regenerator

If the term regarding the magnetocaloric effect is omitted, Eqs. (1-2) represent the behaviour of a passive regenerator. While the implicit model can consider the complete equations, the proposed model neglects the axial conduction in the fluid. In any case, the passive regenerator equations do not have an analytical solution.

Both models have been executed with the parameters given in Table 3 until cyclical steady state is reached, which is when the absolute change in energy of the regenerator from cycle to cycle is below 10^{-4} (Engelbrecht, 2008). The fluid is a mixture of water and ethylene glycol, while the regenerator plates are made of Gd. In this section the specific heat capacity of Gd is considered constant, c_r=300 J kg^{-1} K^{-1}. Laminar flow between infinitely wide parallel plates is assumed in the calculation of the friction factor (f) and the Nusselt number (Nu) (Engelbrecht, 2008). The inlet mass flow rate function is represented in Fig. 8.

Parameter	Value	Parameter	Value
T_H	300 K	T_C	289 K
ρ_f	1033 kg m^{-3}	ρ_r	7901 kg m^{-3}
c_f	3799 J kg^{-1} K^{-1}	c_r	Discussed in text
k_f	0.4808 W m^{-2} K^{-1}	k_r	11 W m^{-2} K^{-1}
μ_f	0.002207 Pa s	H	0.0005 m
ε	0.5	W	0.039 m
Nu	8.24 (Shah and London, 1978)	L	0.080 m

Table 3. Parameters used for regenerator simulations.

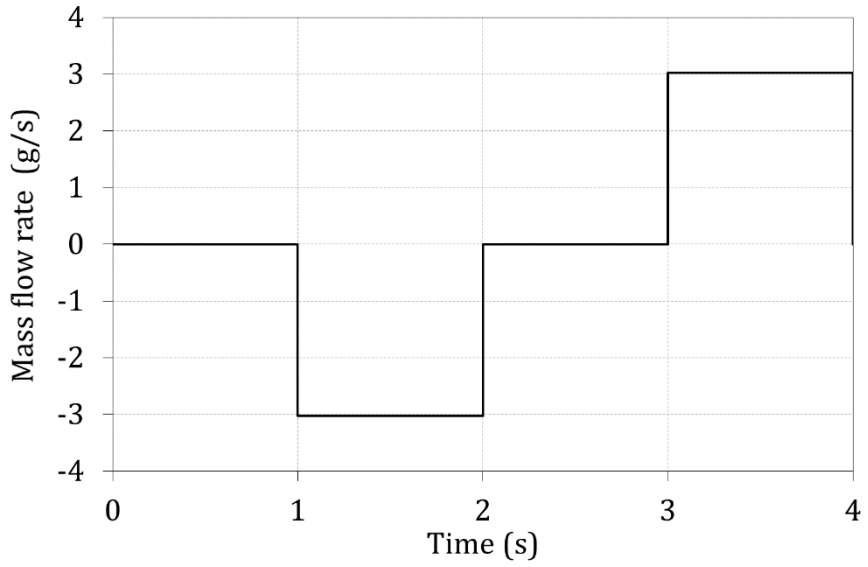

Fig. 8. Inlet mass flow rate in passive regenerator simulations.

Fig. 9 shows the fluid temperature predicted by the models at cyclical steady state. If a fine grid is employed, the maximum fluid temperature difference at the end of the cycle between the two models is 0.025 K. This difference is mainly due to the numerical scheme. In fact, a maximum fluid temperature difference of 0.008 K was obtained between the complete implicit model and neglecting conduction in the fluid.

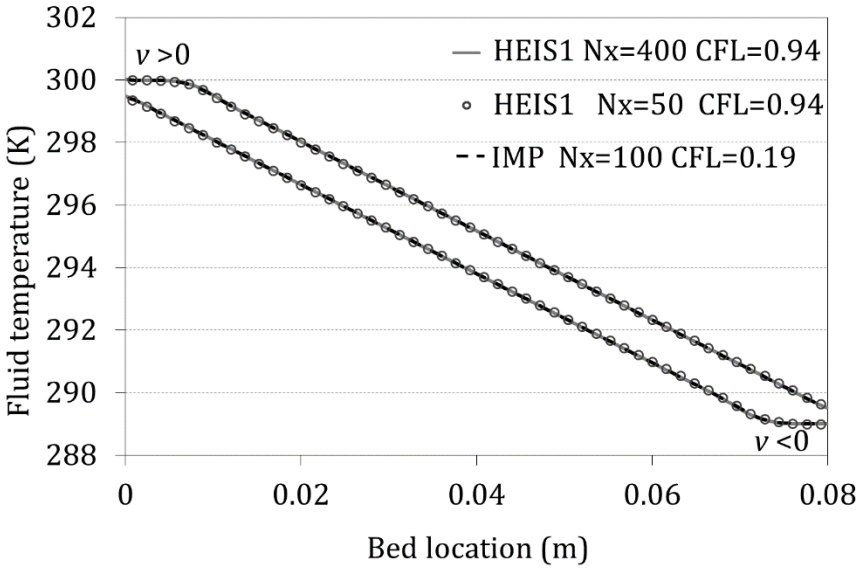

Fig. 9. Predicted fluid temperature at the cyclical steady state in the oscillating passive regenerator.

In order to compare the performance of the schemes, the grid was enlarged. The solution given by the scheme HEIS1 m=0.5 with Nx=400 and CFL=0.94 has been taken as a reference. The proposed scheme with Nx=50 and CFL=0.94 employs 0.41 s per cycle and reproduces the reference solution with a maximum fluid temperature difference of 0.040 K. The implicit scheme needs Nx=100 and CFL=0.19 to achieve a similar accuracy and employs 3.48 s per cycle. As expected from previous results, the numerical dispersion is also reduced with the new scheme (δ_{NS1}=-3.2·10^{-10} while δ_{IMP}=1.9·10^{-9}). Omitting conduction in the fluid in the implicit model leads to similar figures.

These results confirm that axial conduction in the fluid is negligible as supposed in section 2.1. A similar analysis shows that the viscous dissipation term can also be ignored in the studied application. When executing the implicit model with and without this term, the maximum fluid temperature difference is 1.5·10^{-5} K after one cycle and 0.001 K when the cyclical steady state is reached after 261 cycles. Nevertheless, although the influence of the pressure losses in the fluid temperature can be neglected in this case, the pumping power may be a significant part of the total power input to the device and hence play an important role in the efficiency of the AMR operation.

3.5. Active magnetic regenerator (AMR)

The implicit model and the proposed model have been compared under typical AMR working conditions (Engelbrecht et al., 2013). Measured properties of a sample of

commercial grade Gd were integrated in the models as by Lozano et al. (2013). Particularly, c_r and $\partial s_r/\partial \mu_0 H$ are a function of the regenerator temperature and the internal magnetic field. In the implicit model, the changes in the regenerator properties over a small time step are neglected so that the temperatures are calculated using the properties evaluated at the beginning of the time step (Engelbrecht, 2008). For comparison purposes, the same approach has been employed in the presented model.

The models have been run with different levels of discretization employing the parameters in Table 3 until the cyclic steady state is reached. The inlet mass flow rate and the applied magnetic field are synchronized in order to reproduce the AMR cycle (Fig. 10). These inputs are divided in four steps so that each one is reproduced with an exact number of time steps. In this way the inputs remain exactly the same in all the simulations despite the variations of the time grid. Since the main contribution of the model resides in the blow steps (t3 and t4), the number of time steps during the dwell time (t1) and magnetization (t2) was kept constant in this study. During the dwell time the regenerator temperature does not vary significantly, so it was simulated with 2 time steps. On the contrary, the time step during the ramping of the magnetic field has to be small enough so that the former hypothesis on the regenerator properties is valid. In this case, the solution becomes practically independent of the number of time steps if at least 100 time steps are used during t2.

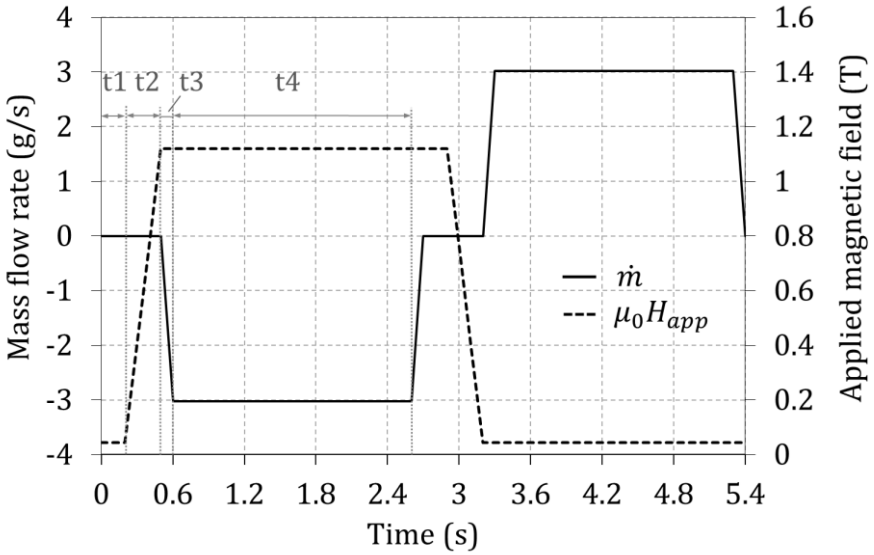

Fig. 10. Inlet mass flow rate and applied magnetic field in AMR simulations.

Fig. 11 shows the fluid temperature profile predicted by the models once the cyclic steady state is reached after 181 cycles. Both schemes reach practically the same results at the different moments of the AMR cycle provided that a sufficient number of nodes

is employed. Compared to the passive regenerator case, finer grids are needed to achieve adequate results due to the temperature dependence of the Gd properties.

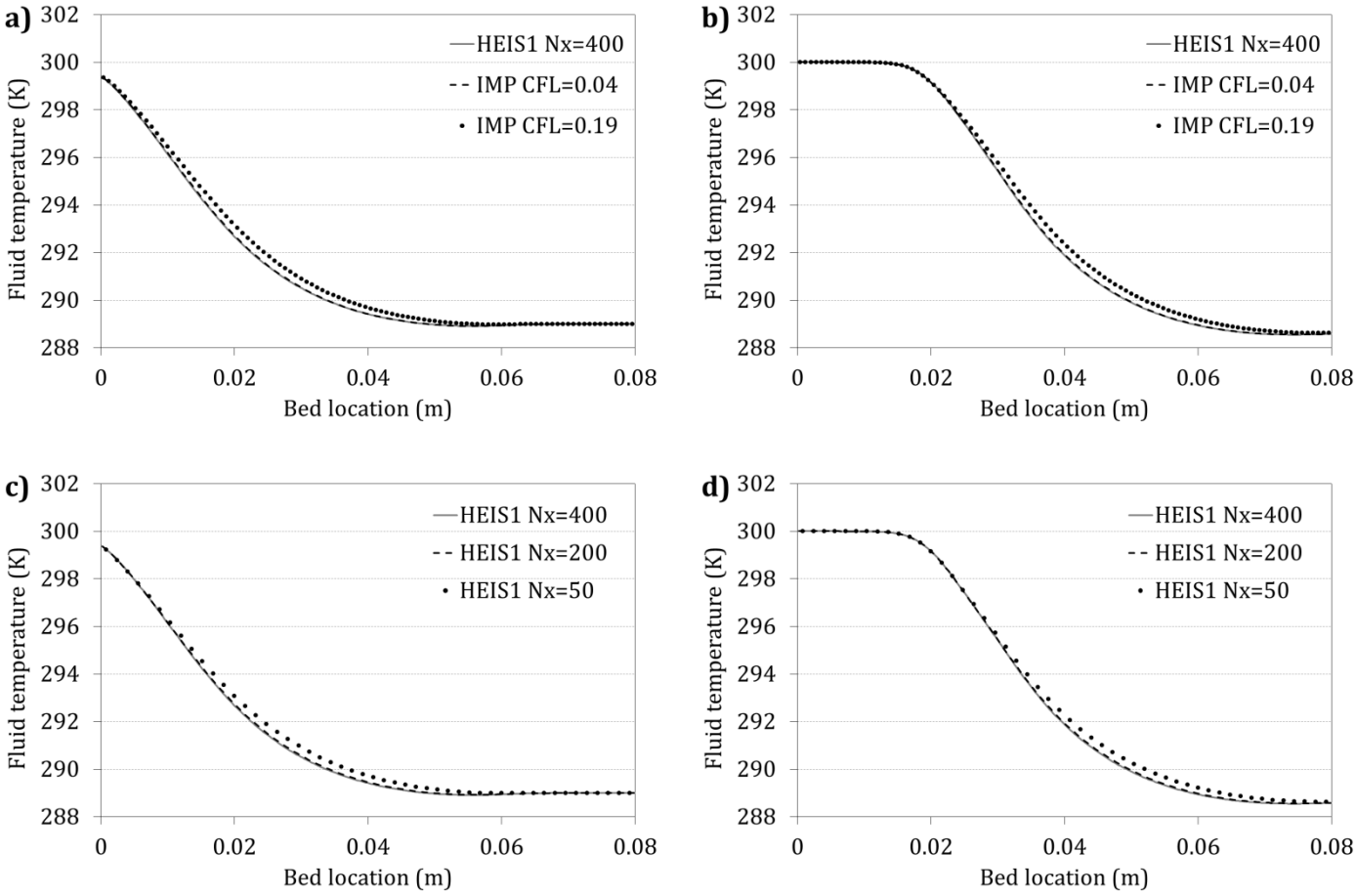

Fig. 11. Predicted fluid temperature at the cyclical steady state in the AMR a) implicit model after the cold blow, b) implicit model after the hot blow, c) HEIS1 m=0.5 after the cold blow and d) HEIS1 m=0.5 after the hot blow.

Table 4 compares the performance of the implicit and the proposed schemes. The $RMSE$ has been calculated taking as a reference the fluid temperature predicted by HEIS1 m=0.5 with Nx=400 and CFL=0.94. While the implicit scheme needs 1100 time steps per blow period (IMP Nx=100 and CFL=0.04) to reproduce the reference solution, the results predicted by the HEIS1 m=0.5 remain practically the same if at least Nx=200 and CFL=0.94 are employed, which means only 88 time steps per blow period. Despite the large number of time steps required to reproduce the magnetization step, the increase in the CFL enabled by the presented scheme and the efficiency of the solution

algorithm results in a significant reduction of the numerical dispersion and the computational time as discussed in sections 3.1 and 3.2.

Scheme	Nx	CFL	$RMSE\ T_f$ (K)	δ (%)	t (s)
IMP	100	0.04	0.0025	$-2.3\cdot10^{-8}$	6726
IMP	100	0.08	0.0090	$-3.0\cdot10^{-8}$	3376
IMP	100	0.19	0.0272	$-1.3\cdot10^{-8}$	1621
HEIS1 m=0.5	400	0.94	ref	$7.3\cdot10^{-9}$	1399
HEIS1 m=0.5	200	0.94	0.0022	$-3.9\cdot10^{-10}$	729
HEIS1 m=0.5	100	0.94	0.0096	$-4.7\cdot10^{-9}$	475
HEIS1 m=0.5	50	0.94	0.0331	$-1.9\cdot10^{-10}$	341

Table 4. AMR simulation results of the proposed model (HEIS) and the implicit model (IMP).

4. Conclusions

A new numerical scheme for the calculation of the conjugate heat transfer in parallel-plate active magnetic regenerators (AMR) has been developed, based on a combination of explicit and implicit numerical techniques tailored to the heat transfer phenomena that prevail in the regenerator bed. Compared to the most commonly employed fully implicit scheme, the new hybrid explicit-implicit scheme (HEIS) prevents numerical diffusion and oscillations, achieving conservation and monotonicity with less computational effort while preserving and even improving the accuracy of the numerical solution.

A thorough validation has been carried out to test the performance of the new scheme. The HEIS reproduces very accurately the transport equation and also the ideal regenerator cases with analytical solution requiring less spatial nodes and in general much lower computational time than the fully implicit scheme. For the same number of spatial nodes, the latter requires a very small time step and consequently works with a very low value of the *CFL*, which causes numerical dispersion in the simulation of transport phenomena. The HEIS enables the use of a time step as large as *CFL*=1, thus reducing the numerical error and the computational time. The HEIS further enhances the simulation time by adopting the tri-diagonal matrix algorithm to solve the system of equations, which is more computationally efficient than the matrix inversion method required by the fully implicit scheme.

Similar conclusions are obtained when comparing the schemes in the regenerator cases without analytical solution, for which both methods reach practically the same numerical solution. Besides improving the numerical dispersion, the HEIS can reduce the computational time by 88% in the simulation of the oscillating passive regenerator and by 89% in the case of the AMR, which requires finer grids due to the strong variation of the regenerator properties with the temperature.

Acknowledgements

B. Torregrosa-Jaime acknowledges the Spanish Ministry of Education, Culture and Sport (Ministerio de Educación, Cultura y Deporte) for receiving the Research Fellowship FPU ref. AP2010-2160.

References

Bahl, C.R.H., Petersen, T.F., Pryds, N., Smith, A., 2008. A versatile magnetic refrigeration test device. Rev. Sci. Instrum. 79, 093906.

Dikeos, J. and Rowe, A., 2013. Validation of an active magnetic regenerator test apparatus model. Int. J. Refrigeration 36, 921-931.

Dragutinovic, G.D. and Baclic, B.S., 1998. Operation of Counterflow Regenerators, Computational Mechanics Inc., Billerica, MA.

Engelbrecht, K., 2008. A Numerical Model of an Active Magnetic Regenerator Refrigerator with Experimental Validation. PhD Thesis, University of Wisconsin-Madison, Madison, WI.

Engelbrecht, K., Tušek, J., Nielsen, K.K., Kitanovski, A., Bahl, C.R.H., Poredoš, A., 2013. Improved modelling of a parallel plate active magnetic regenerator. J. Phys. D: Appl. Phys. 46, 255002.

Incropera, F.P., Dewitt, D.P., Bergman, T.L., Lavine, A.S., 2007. Fundamentals of Heat and Mass Transfer, sixth ed. John Wiley & Sons, Hoboken.

Klein, H. and Eigenberger, G., 2001. Approximate solutions for metallic regenerative heat exchangers. Int. J. Heat Mass Transfer 44, 3553-3563.

Lozano, J.A., Engelbrecht, K., Bahl, C.R.H., Nielsen, K.K., Eriksen, D., Olsen, U.L., Barbosa Jr., J.R., Smith, A., Prata, A.T., Pryds, N., 2013. Performance analysis of a rotary active magnetic refrigerator. Appl. Energy 111, 669-680.

Nellis, G.F. and Klein, S.A., 2006. Regenerative heat exchangers with significant entrained fluid heat capacity. Int. J. Heat Mass Transfer 49, 329-340.

Nielsen, K.K., Bahl, C.R.H., Smith, A., Bjørk, R., Pryds, N., Hattel, J., 2009. Detailed numerical modeling of a linear parallel-plate Active Magnetic Regenerator. Int. J. Refrigeration 32, 1478-1486.

Nielsen, K.K., Tusek, J., Engelbrecht, K., Schopfer, S., Kitanovski, A., Bahl, C.R.H., Smith, A., Pryds, N., Poredos, A., 2011. Review on numerical modeling of active magnetic regenerators for room temperature applications. Int. J. Refrigeration 34, 603-616.

Nielsen, K.K. and Engelbrecht, K., 2012. The influence of the solid thermal conductivity on active magnetic regenerators. J. Phys. D: Appl. Phys. 45, 145001.

Nikkola, P., Mahmed, C., Balli, M., Sari, O., 2014. 1D model of an active magnetic regenerator. Int. J. Refrigeration 37, 43-50.

Oliveira, P.A., Trevizoli, P.V., Barbosa Jr., J.R., Prata, A.T., 2012. A 2D hybrid model of the fluid flow and heat transfer in a reciprocating active magnetic regenerator. Int. J. Refrigeration 35, 98-114.

Petersen, T.F., 2007. Numerical modelling and analysis of a room temperature magnetic refrigeration system. PhD Thesis, Risø National Laboratory, Technical University of Denmark, Roskilde.

Petersen, T.F., Engelbrecht, K., Bahl, C.R.H., Elmegaard, B., Pryds, N., Smith, A., 2008. Comparison between a 1D and a 2D numerical model of an active magnetic regenerative refrigerator. J. Phys. D: Appl. Phys. 41, 105002.

Romero Gómez, J., Ferreiro Garcia, R., Carbia Carril, J., Romero Gómez, M., 2013. A review of room temperature linear reciprocating magnetic refrigerators. Renewable and Sustainable Energy Reviews 21, 1-12.

Shah, R.K. and London, A.L., 1978. Laminar Flow Forced Convection in Ducts, Academic Press, New York.

Shitzer, A. and Levy, M., 1983. Transient Behavior of a Rock-Bed Thermal Storage System Subjected to Variable Inlet Air Temperatures: Analysis and Experimentation. J. Sol. Energy Eng. 105, 200-206.

Trevizoli, P.V., Barbosa Jr., J.R., Ferreira, R.T.S., 2011. Experimental evaluation of a Gd-based linear reciprocating active magnetic regenerator test apparatus. Int. J. Refrigeration 34, 1518-1526.

Tušek, J., Kitanovski, A., Poredoš, A., 2013. Geometrical optimization of packed-bed and parallel-plate active magnetic regenerators. Int. J. Refrigeration 36, 1456-1464.

Tušek, J., Kitanovski, A., Prebil, I., Poredoš, A., 2011. Dynamic operation of an active magnetic regenerator (AMR): Numerical optimization of a packed-bed AMR. Int. J. Refrigeration 34, 1507-1517.

Van Leer, B., 1977. Towards the ultimate conservative difference scheme III. Upstream-centered finite-difference schemes for ideal compressible flow. Journal of Computational Physics 23, 263-275.